Supplementary Information

Anisotropic supramolecular plastics prepared from an undercooled liquid crystalline phase of a cholesterol-based low-molecular-weight compound

Chia-Hsin Cheng, Yuichiro Watanabe, Takashi Kajitani, Sadaki Samitsu, Kazunori Sugiyasu*

* E-mail: sugiyasu.kazunori.8z@kyoto-u.ac.jp

Table of Contents

S1. Supplementary methods

S1a. General methods

Nuclear magnetic resonance (NMR) spectra were recorded on a JNM-ECZ400S spectrometer (400 MHz). All chemical shifts are reported in parts per million (ppm) from tetramethylsilane (0 ppm for ^{1}H), residual $CHCl_3$ (77 ppm for ^{13}C) as internal standards. Electrospray ionization mass spectra (ESI-MS) were obtained using a Thermo Fisher Scientific Exactive Plus instrument. Samples were dissolved in a 1:1 (v/v) mixture of $CHCl_3$ and MeOH prior to measurement. Thermal analyses were conducted on a Netzsch STA 2500 Regulus and a Netzsch DSC 300 Caliris equipped with a cooling accessory under a nitrogen atmosphere. Characteristic textures of the LC phases were examined using an Olympus BX53-P polarizing microscope equipped with a Linkam 10083L heating stage. X-ray diffraction (XRD) patterns of samples were measured using a Rigaku NANOPIX equipped with a HyPix-6000 detector. For temperature-dependent measurements, a Linkam HSFX350-GI heating stage was used. The scattering vector ($q = 4\pi\sin\theta/\lambda$), scattering angle θ, and the position of the incident X-ray beam on the detector were calibrated using several orders of layer reflections from silver behenate (d = 58.380 Å), where λ refers to the wavelength of the X-ray beam (Cu Kα, 1.54 Å). The sample-to-detector distance was approximately 300 mm. Using the Rigaku 2DP software, the obtained diffraction patterns were integrated along the Debye–Scherrer rings to afford 1D intensity data. Temperature-dependent Fourier-transform infrared (FT-IR) spectra were collected using a PerkinElmer Spectrum Two FT-IR spectrometer equipped with an Instec mK1000 controller attached to a HCS402 heating stage. Polarized FT-IR spectra were acquired on a Thermo Fisher Scientific Nicolet iS50 FT-IR spectrometer. Alignment of molecules in supramolecular plastic sheets was examined under crossed Nicols by polarizing films (Narika Co., Ltd.) on an LED light tracing board (Figure 3f,k in the main text). Viscosities were measured using an Anton Paar MCR 302e rheometer with a measuring cone CP25-2. Pressing process was performed using an Imoto Machinery Co., Ltd. IMC-11FD hydraulic press machine. Evolution of selective reflection was monitored using a JASCO J-820 spectropolarimeter. Colour information in the real-time video was analyzed by ImageJ (Fiji). Extrusion process was performed using a Shimadzu CFT-500EX flow tester. Tensile, compression, and three-point flexural tests were performed using a Shimadzu AGS-X universal testing machine. Fractured morphology was examined using a Leica Ivesta 3 Greenough stereo microscope.

S1b. Melt-moulding method

Chol-C_{12}, candle wax, soap, and low-density polyethylene (LDPE) samples were placed in rectangular silicone moulds (L40 mm × W20 mm). The moulds were heated at 100 °C to melt the materials (LDPE was processed at 160 °C due to its higher melting point). After melting, the materials were cooled and solidified in an incubator (25°C) for 24 h, yielding bulk samples with a thickness of 6.6 ± 0.65 mm.

S1c. Sample preparation for time-dependent XRD measurements

The procedure was similar to the preparation of supramolecular plastic sheets. In this case, four PET films were used (two small pieces and two larger pieces). The metastable LC **Chol-C$_{12}$** sample was sandwiched between the two small pieces, then further laminated between two larger pieces. The stacked assembly was pressed at room temperature for 10 s. After pressing, the two small pieces were peeled off and directly mounted onto a sample holder, followed by measurements performed at room temperature.

S1d. Filament extrusion method

1.0 g of **Chol-C$_{12}$** was melted in a silicone mould at 100 °C and subsequently quenched on an aluminum block cooled in a liquid nitrogen bath for 50 s. The resulting sample was then loaded into flow tester and incubated for 4 min at 25 °C prior to extrusion. The sample was first compacted pneumatically, followed by pre-extrusion using a 0.5 kg load for 15 s to form a leading filament. Subsequently, a 30 kg load was applied to extrude the remaining **Chol-C$_{12}$**, yielding an anisotropic filament.

S2. Materials and synthesis

S2a. Materials

(3β)-cholest-5-en-3-yl chloroformate (TCI Chemicals, 98%), hexan-1-amine (TCI Chemicals, 99%), dodecan-1-amine (TCI Chemicals, 97%), octadecan-1-amine (TCI Chemicals, 85%), *N*,*N*-diethylethanamine (Et_3N, TCI Chemicals, 99%), anhydrous dichloromethane (CH_2Cl_2, Kanto Chemicals, 99.5%), and anhydrous sodium sulfate (Na_2SO_4, Wako Chemicals, 99%) were used as received without further purification.

For the pressing process, poly(ethylene terephthalate) (PET) films (PET75X1-K-ASI5, 75 μm thickness; Tokyo Film Service Co., Ltd.), silicon mould (Daiso) were used as received. Water-sensitive reactions were conducted under a nitrogen atmosphere using anhydrous solvents.

S2b. Synthesis of Chol-C_6

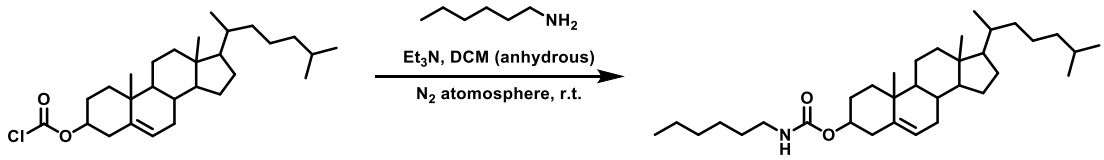

Scheme S1. Synthetic route to **Chol-C_6**

A solution of (3β)-cholest-5-en-3-yl chloroformate (8.8 g, 19.6 mmol, 1 eq.) in anhydrous CH_2Cl_2 (70 mL) was dropwise added to a stirred solution of hexan-1-amine (2.2 g, 21.5 mmol, 1.1 eq) and Et_3N (4.4 g, 43.1 mmol, 2.2 eq.) in anhydrous CH_2Cl_2 (105 mL) at 0 °C under a nitrogen atmosphere. The mixture was stirred at room temperature for 4 h. The mixture was then washed with brine (100 mL) twice and dried over anhydrous Na_2SO_4. The filtrate was evaporated, and the solid residue was purified through column chromatography (silica gel, hexane/EtOAc = 20:1 v/v, R_f = 0.30) to yield compound **Chol-C_6** as a white solid (9.6 g, yield = 95%).

^{1}H NMR (400 MHz, $CDCl_3$, 298 K): δ (ppm) = 5.37-5.35 (m, 1H$_a$), 4.55-4.45 (m, 1H$_b$ & 1H$_c$), 3.14 (q, J = 6.4 Hz, 2H$_d$), 2.37-0.74 (m, 51H$_e$), 0.68 (s, 3H$_f$) as shown in **Supplementary Fig. 1.**; ^{13}C NMR (100 MHz, $CDCl_3$, 298K): δ (ppm) = 156.2, 140.0, 122.5, 77.4, 77.1, 76.8, 74.2, 56.8, 56.2, 50.1, 42.4, 41.0, 39.8, 39.6, 38.7, 37.1, 36.6, 36.3, 35.9, 32.0, 32.0, 31.6, 30.1, 28.3, 28.3, 28.1, 26.5, 24.4, 23.9, 22.9, 22.6, 21.1, 19.4, 18.8, 14.1, 11.9 as shown in **Supplementary Fig. 2.**; m.p. 87 °C; HRMS (ESI, MeOH/$CHCl_3$ = 1/1): m/z $[M+Na]^+$ calcd. for $C_{34}H_{59}NO_2$ 536.4438, observed 536.4431.

S2c. Synthesis of Chol-C_{12}

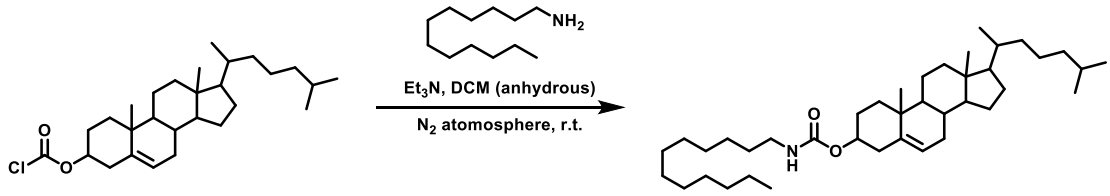

Scheme S2. Synthetic route to **Chol-C_{12}**

A solution of (3β)-cholest-5-en-3-yl chloroformate chloroformate (7.5 g, 16.7 mmol, 1 eq.) in anhydrous CH_2Cl_2 (70 mL) was dropwise added to a stirred solution of dodecan-1-amine (3.4 g, 18.4 mmol, 1.1 eq) and Et_3N (3.7 g, 36.7 mmol, 2.2 eq.) in anhydrous CH_2Cl_2 (105 mL) at 0 °C under a nitrogen atmosphere. The mixture was stirred at room temperature for 4 h. The mixture was then washed with brine (100 mL) twice and dried over anhydrous Na_2SO_4. The filtrate was evaporated, and the solid residue was purified through column chromatography (silica gel, hexane/EtOAc = 20:1 v/v, R_f = 0.33) to yield compound **Chol-C_{12}** as a white solid (9.4 g, yield = 94%).

S2d. Synthesis of Chol-C_{12} without using column chromatography

The procedure is analogous to the synthesis of **Chol-C_{12}** (see above) but in a 14-gram scale. The solid residue was dissolved in hexane/EtOAc (20:1 v/v, 200 mL) and mixed with silica powder, and the resulting suspension was stirred for 30 min. The mixture was filtered to remove the silica, and the silica cake was washed with EtOAc (200 mL) twice. The combined filtrates were concentrated to yield compound **Chol-C_{12}** as a white solid (13.7 g, yield = 97%).

^{1}H NMR (400 MHz, $CDCl_3$, 298K): δ (ppm) = 5.36-5.35 (m, 1H_a), 4.55-4.45 (m, 1H_b & 1H_c), 3.14 (q, J = 6.4 Hz, 2H_d), 2.37-0.81 (m, 63H_e), 0.66 (s, 3H_f) as shown in **Supplementary Fig. 3.**; ^{13}C NMR (100 MHz, $CDCl_3$, 298K): δ (ppm) = 156.2, 140.0, 122.5, 77.4, 77.1, 76.8, 74.2, 56.8, 56.2, 50.1, 42.4, 41.0, 39.8, 39.6, 38.7, 37.1, 36.6, 36.3, 35.9, 32.0, 32.0, 30.1, 29.7, 29.7, 29.6, 29.4, 29.4, 28.3, 28.3, 28.1, 26.8, 24.4, 23.9, 22.9, 22.8, 22.6, 21.1, 19.4, 18.8, 14.2, 11.9 as shown in **Supplementary Fig. 4.**; m.p. 78 °C.; HRMS (ESI, MeOH/$CHCl_3$ = 1/1): *m/z* $[M+Na]^+$ calcd. for $C_{40}H_{71}NO_2$ 620.5377, observed 620.5371.

S2e. Synthesis of Chol-C_{18}

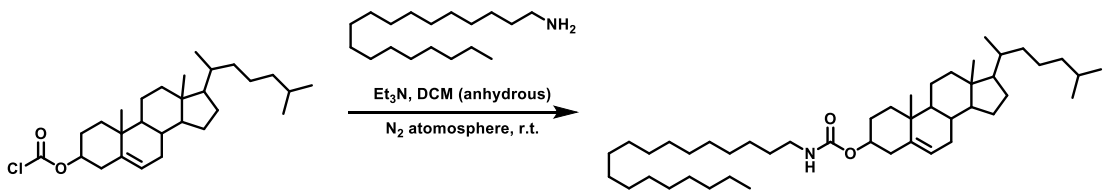

Scheme S3. Synthetic route to **Chol-C_{18}**

A solution of (3β)-cholest-5-en-3-yl chloroformate (7.0 g, 15.6 mmol, 1 eq.) in anhydrous CH_2Cl_2 (70 mL) was dropwise added to a stirred solution of octadecan-1-amine (4.6 g, 17.1 mmol, 1.1 eq) and Et_3N (3.5 g, 34.2 mmol, 2.2 eq.) in anhydrous CH_2Cl_2 (105 mL) at 0 °C under a nitrogen atmosphere. The mixture was stirred at room temperature for 4 h. The mixture was then washed with brine (100 mL) twice and dried over anhydrous Na_2SO_4. The filtrate was evaporated, and the solid residue was purified through column chromatography (silica gel, hexane/EtOAc = 20:1 v/v, R_f = 0.35) to yield compound **Chol-C_{18}** as a white solid (9.7 g, yield = 91%).

^{1}H NMR (400 MHz, $CDCl_3$, 298K): δ (ppm) = 5.36-5.35 (m, 1H_a), 4.54-4.48 (m, 1H_b & 1H_c), 3.14 (q, J = 6.6 Hz, 2H_d), 2.37-0.84 (m, 77H_e), 0.66 (s, 3H_f) as shown in **Supplementary Fig. 5.**; ^{13}C NMR (100 MHz, $CDCl_3$, 298K): δ (ppm) = 156.2, 140.0, 122.5, 77.4, 77.1, 76.8, 74.2, 56.8, 56.2, 50.1, 42.4, 41.0, 39.8, 39.6, 38.7, 37.1, 36.6, 36.3, 35.9, 32.0, 32.0, 32.0, 30.1, 29.8, 29.7, 29.6, 29.5, 29.4, 28.3, 28.3, 28.1, 26.8, 24.4, 23.9, 22.9, 22.8, 22.6, 21.1, 19.4, 18.8, 14.2, 11.9 as shown in **Supplementary Fig. 6.**; m.p. 81 °C; HRMS (ESI, MeOH/$CHCl_3$ = 1/1): *m/z* $[M+Na]^+$ calcd. for $C_{46}H_{83}NO_2$ 704.6316, observed 704.6310.

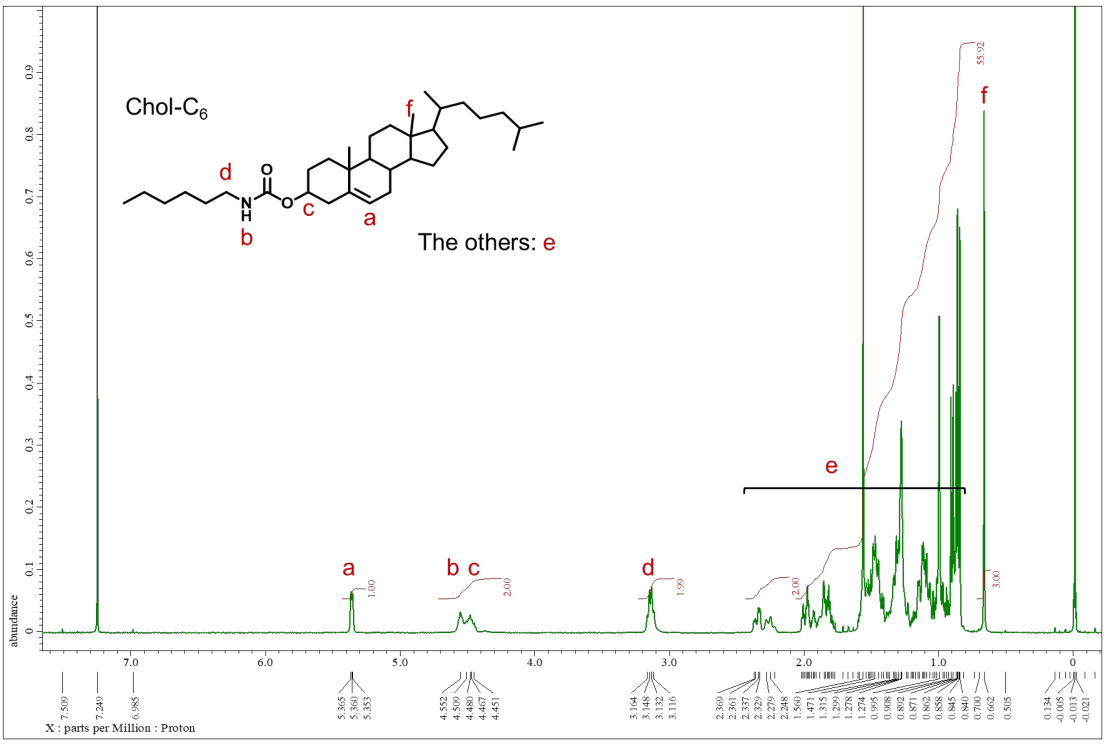

Supplementary Fig. 1.
^{1}H NMR (400 MHz) spectrum of **Chol-C$_6$** in $CDCl_3$ at 298 K.

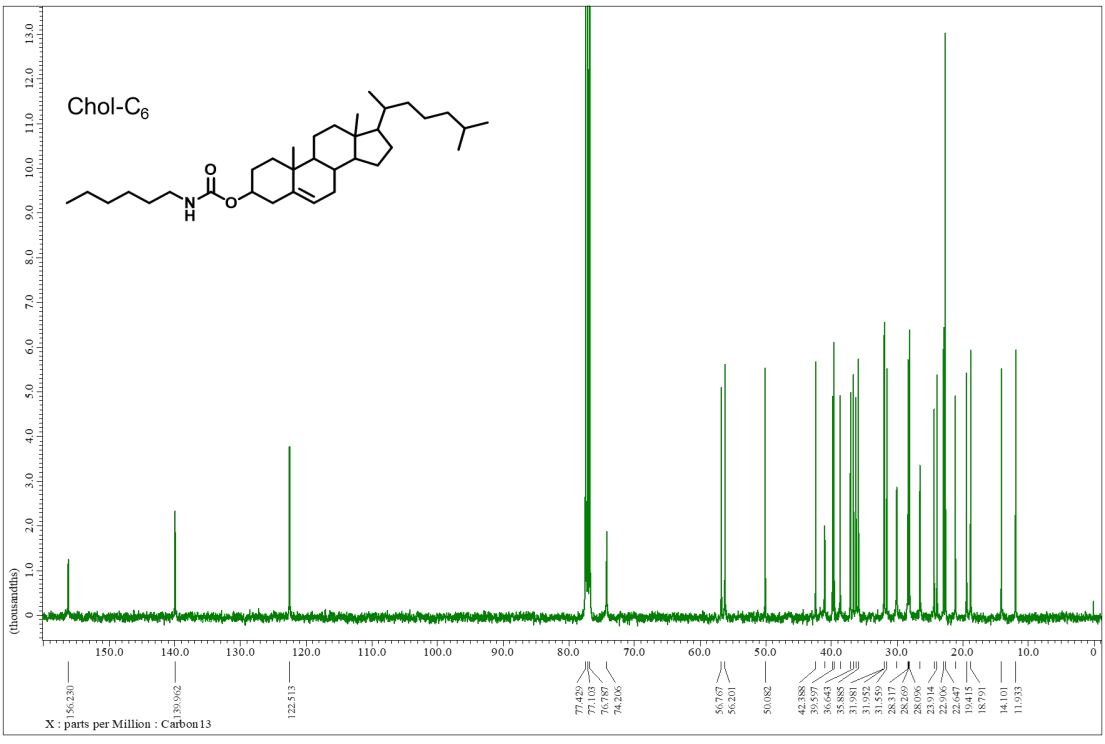

Supplementary Fig. 2.
^{13}C NMR (100 MHz) spectrum of **Chol-C$_6$** in $CDCl_3$ at 298 K.

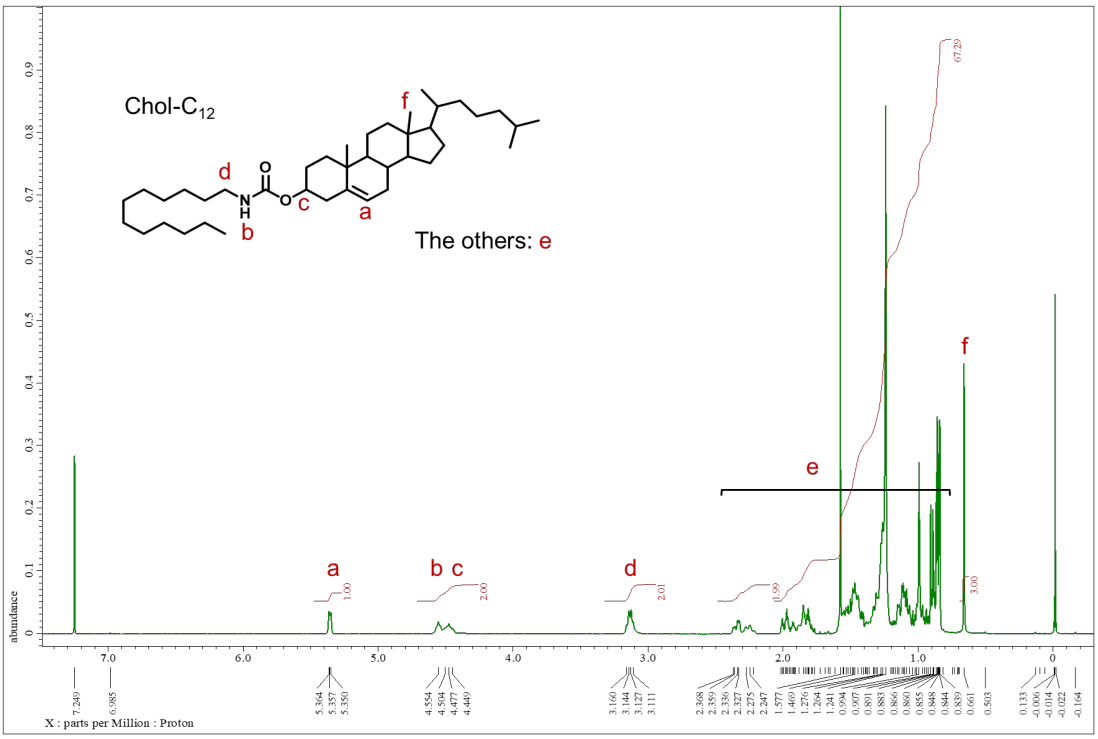

Supplementary Fig. 3.
^{1}H NMR (400 MHz) spectrum of **Chol-C$_{12}$** in $CDCl_3$ at 298 K.

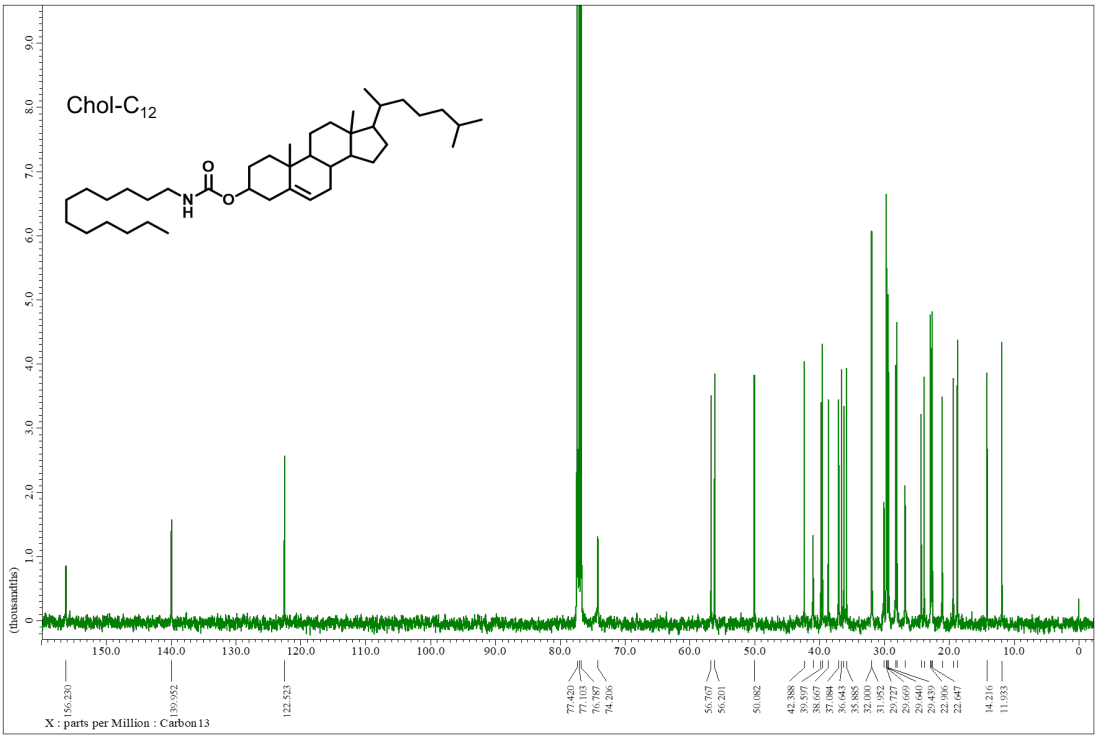

Supplementary Fig. 4.
^{13}C NMR (100 MHz) spectrum of **Chol-C$_{12}$** in $CDCl_3$ at 298 K.

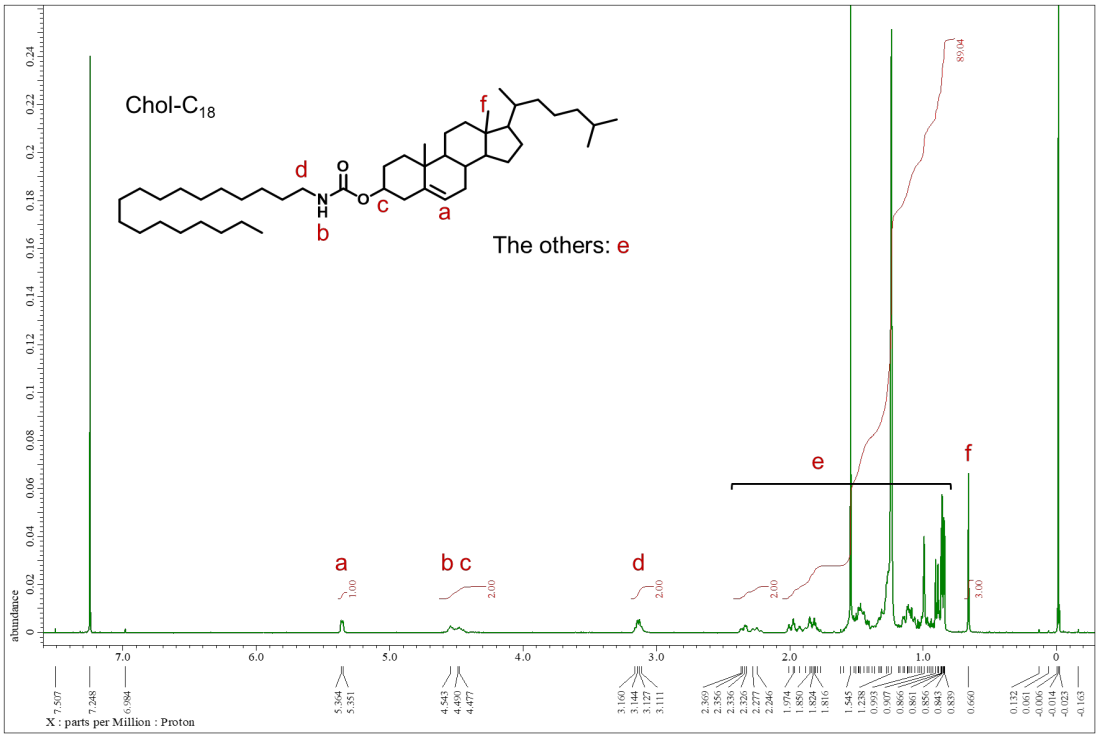

Supplementary Fig. 5.
^{1}H NMR (400 MHz) spectrum of **Chol-C$_{18}$** in $CDCl_3$ at 298 K .

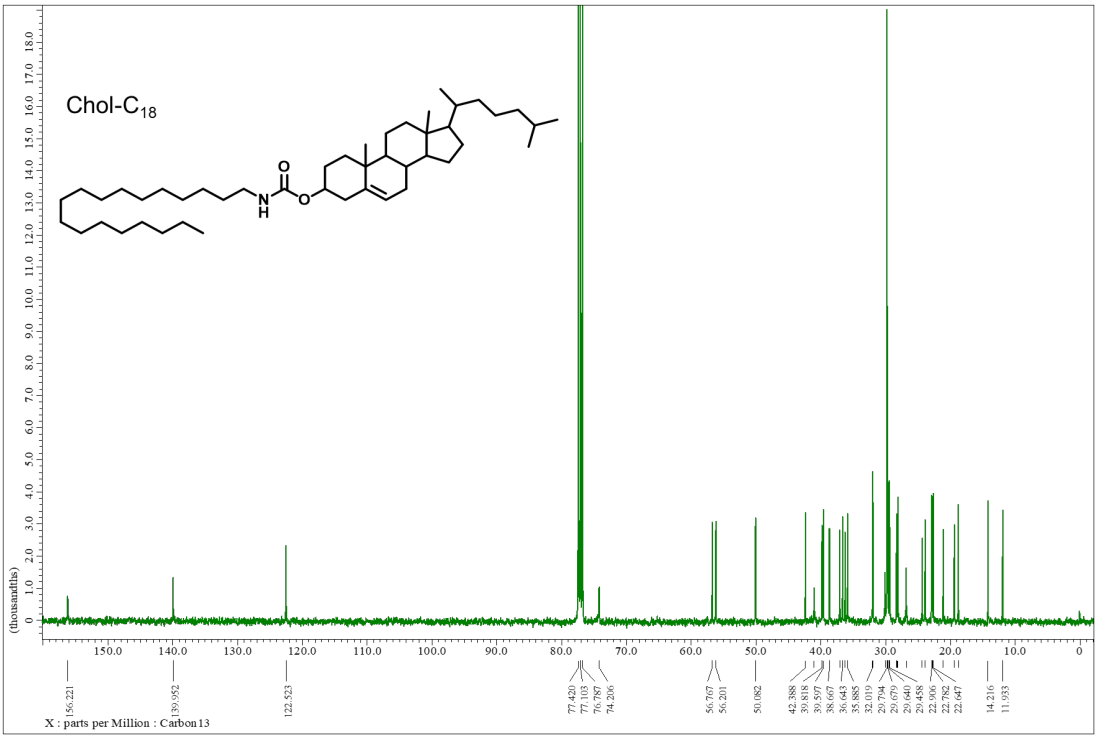

Supplementary Fig. 6.
^{13}C NMR (100 MHz) spectrum of **Chol-C$_{18}$** in $CDCl_3$ at 298 K.

S3. Supplementary figures

S3a. Thermogravimetric analysis (TGA)

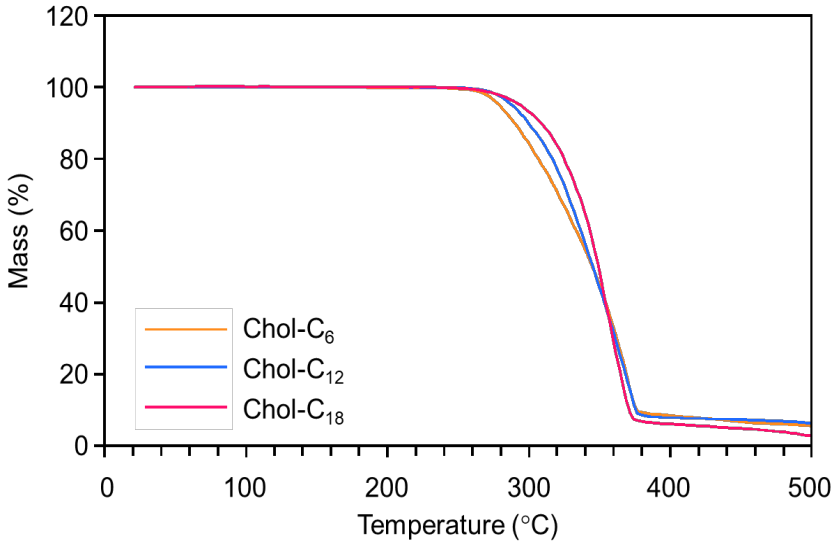

Supplementary Fig. 7.
TGA curves of **Chol-C_6**, **Chol-C_{12}**, and **Chol-C_{18}** from 25 to 500 °C obtained at a rate of 10 °C/min under a N_2 atmosphere.

S3b. Characteristic texture observed using polarized optical microscopy (POM)
After melting, the samples were cooled from 90 °C to 0 °C at a rate of 10 °C/min, and images were acquired at 10 °C intervals. In the isotropic molten state (90 °C), both **Chol-C_6** and **Chol-C_{12}** appeared completely dark under crossed Nicols. Upon cooling, characteristic textures emerged, indicating that **Chol-C_6** and **Chol-C_{12}** formed LC phases.

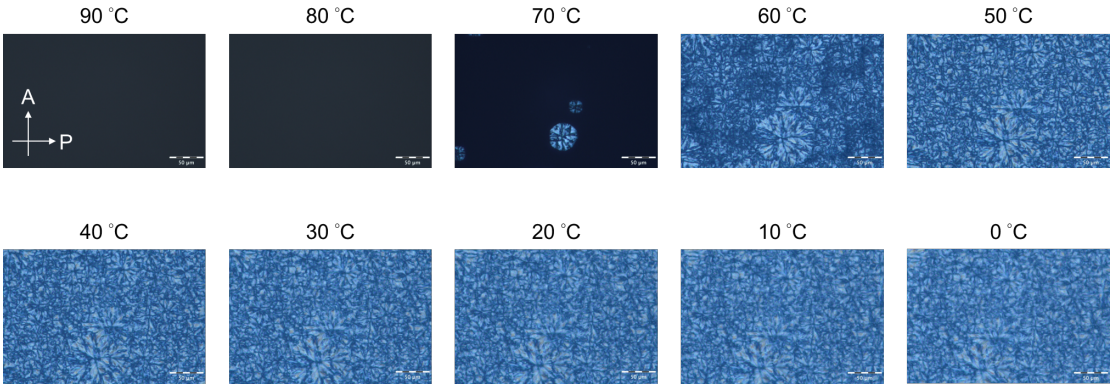

Supplementary Fig. 8.
Polarized optical microscopy images of **Chol-C_6** from 90 ºC to 0 ºC at a rate of 10 °C/min under a N_2 atmosphere: scale bar = 50 µm.

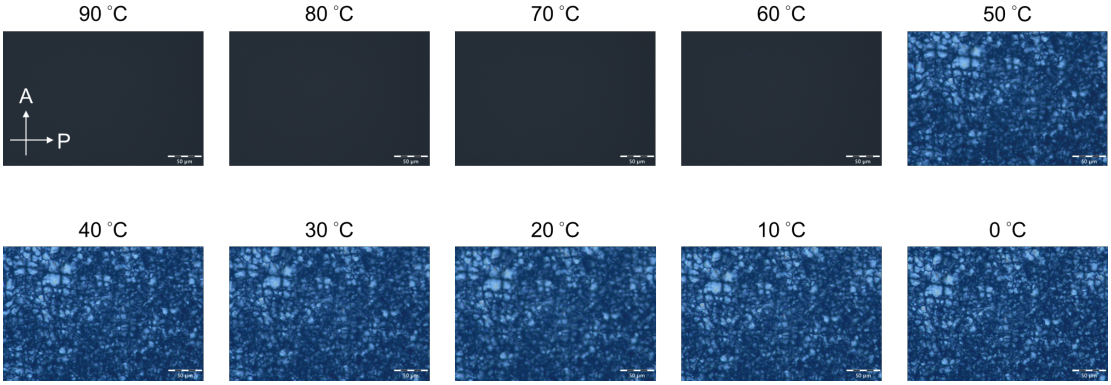

Supplementary Fig. 9.
Polarized optical microscopy images of **Chol-C_{12}** from 90 ºC to 0 ºC at a rate of 10 °C/min under a N_2 atmosphere: scale bar = 50 µm.

S3c. Temperature-dependent FT-IR spectra of methylene stretching

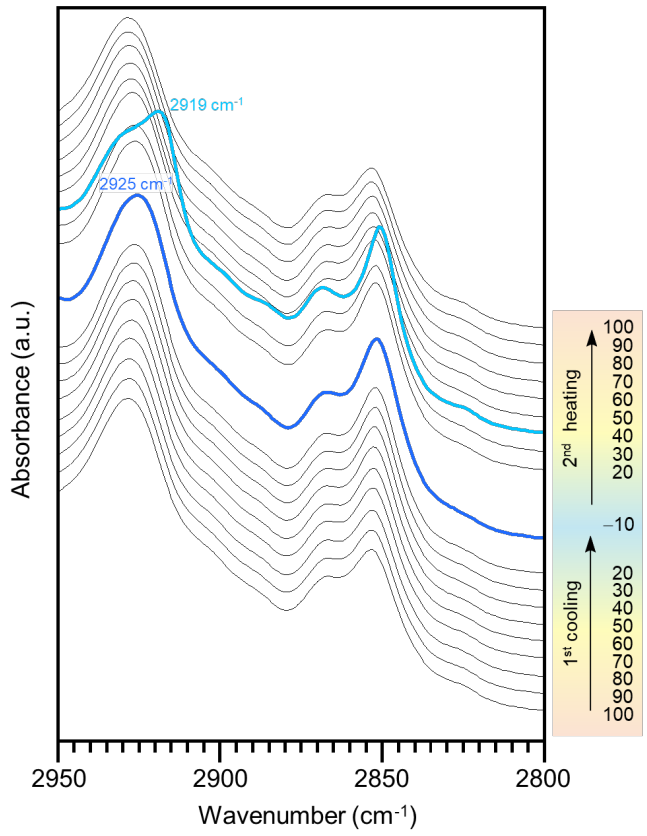

Supplementary Fig. 10.
Temperature-dependent FT-IR spectra of **Chol-C_{12}** in the range of 2950 to 2800 cm^{-1} obtained during cooling from 100 to −10 °C, followed by reheating to 100 °C.

S3d. Temperature-dependent XRD profiles and FT-IR spectra

The phases transitions of **Chol-C$_6$**, **Chol-C$_{12}$**, and **Chol-C$_{18}$** were examined across temperatures. For XRD and FT-IR measurements, the samples were placed in capillaries or on a sapphire substrate, respectively, and subjected to controlled temperature variations. After reaching the thermal equilibrium at designated temperatures, measurements were conducted. As shown in **Supplementary Fig. 11**, **Chol-C$_6$** remained its nematic LC phase while cooling to –10 °C. In contrast, as shown in **Supplementary Fig. 12**, **Chol-C$_{18}$** started forming lamellar crystalline structures when cooled to 50 °C. Correspondingly, a blue shift in the N–H stretching vibration was observed in the FT-IR spectra, consistent with the weakening of hydrogen bonding accompanying the enhanced packing of cholesteryl groups as is the case of **Chol-C$_{12}$**.

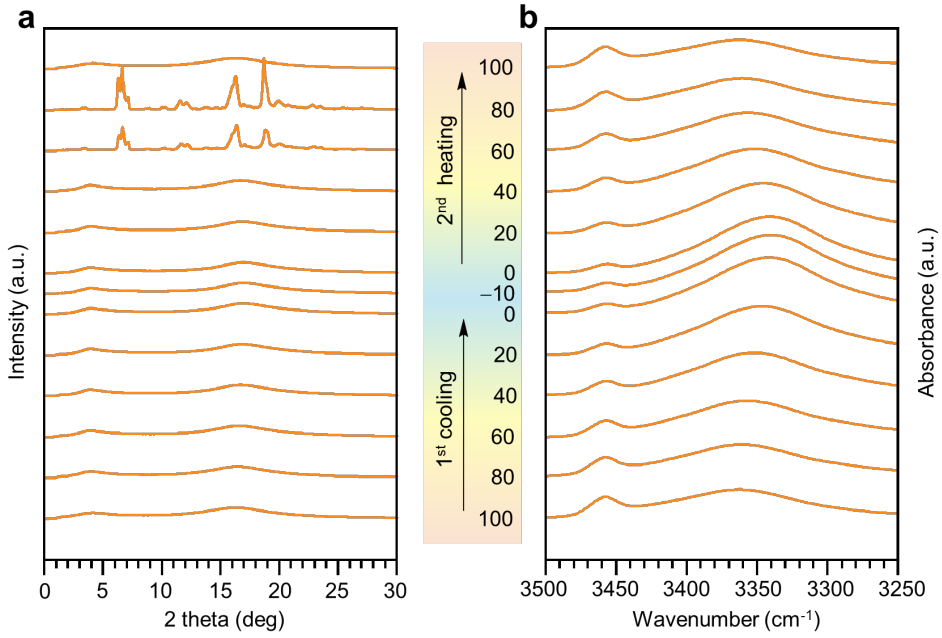

Supplementary Fig. 11.

Temperature-dependent XRD profiles and FT-IR spectra of **Chol-C$_6$** obtained during cooling from 100 to −10 °C, followed by reheating to 100 °C.

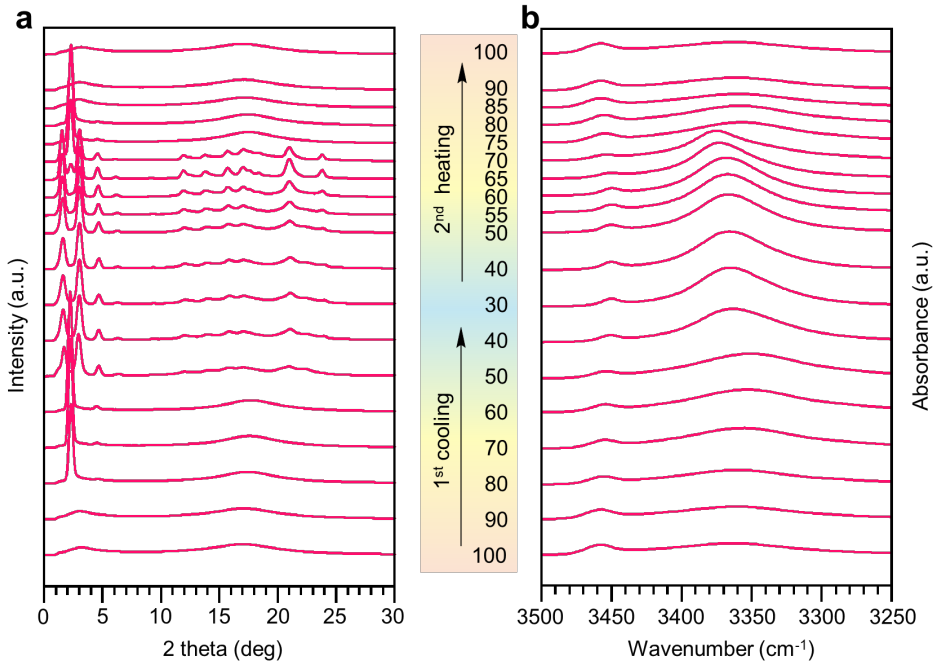

Supplementary Fig. 12.
Temperature-dependent XRD profiles and FT-IR spectra of **Chol-C_{18}** obtained during cooling from 100 to 30 °C, followed by reheating to 100 °C.

S3e. Quenching temperature effect

A **Chol-C$_{12}$** sample was first melted by heating to 100 °C to eliminate thermal history if any. The sample was then quenched at a cooling rate of −50 °C/min to designated temperatures (–50 to 25 °C) and held for 5 min for reaching thermal equilibrium. The crystallization behaviour was monitored in the following heating trace (10 °C/min).

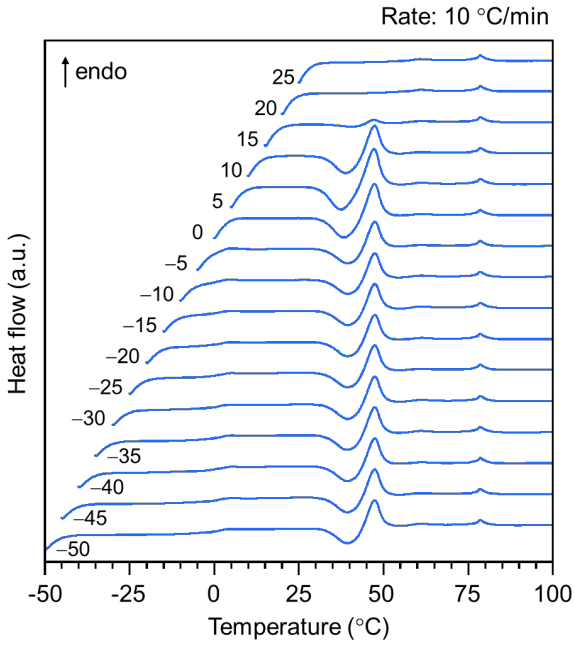

Supplementary Fig. 13.
DSC curves of **Chol-C$_{12}$** from each quenched temperature to 100 °C at a rate of 10 °C/min under a N_2 atmosphere.

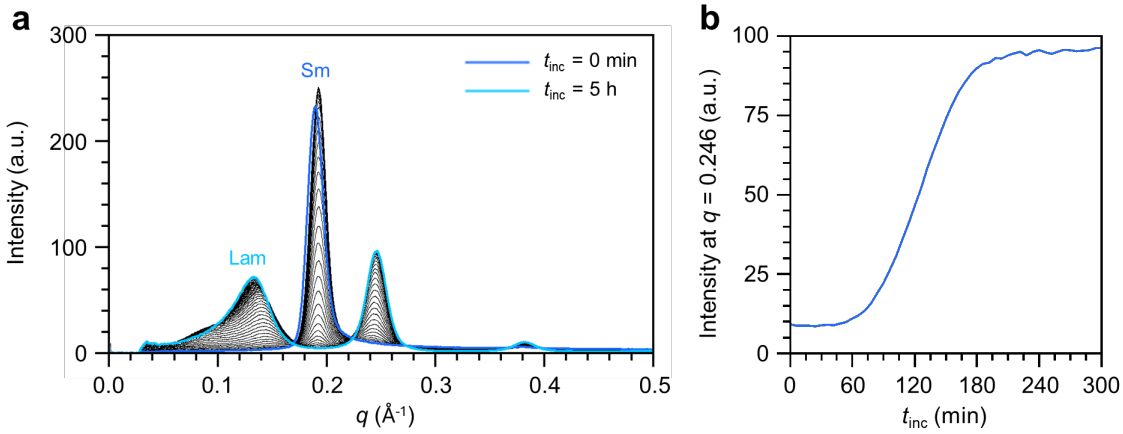

Supplementary Fig. 14.
a, Time-dependent XRD profiles of **Chol-C$_{12}$** recorded at 6-min intervals from 0 min to 5 h. **b**, A change in the diffraction intensity at q = 0.246 as a function of time.

S3f. Incubating temperature effect

A **Chol-C$_{12}$** sample was first melted by heating to 100°C to eliminate thermal history if any. It was then rapidly cooled to −50 °C at a rate of −50 °C/min and held for 10 min for reaching thermal equilibration. Subsequently, the temperature was raised to the designated incubation temperatures (22 to 36 °C) at a heating rate of 50 °C/min, and the crystallization behaviour was monitored in the ensuing isothermal stage.

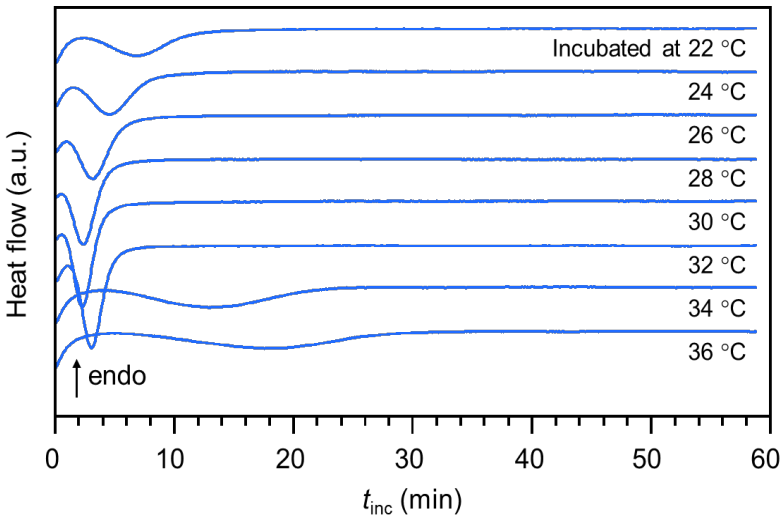

Supplementary Fig. 15.
Isothermal DSC curves of **Chol-C$_{12}$** obtained at various incubation temperatures ranging from 22 °C to 36 °C for 1 h.

The degree of crystallinity was evaluated from the integrated area of the exothermic peak obtained from isothermal DSC traces. The Avrami plot was then constructed from the crystallization conversion (**Supplementary Fig. 16**), which was evaluated from the degree of crystallinity.[S1] To calculate the area of crystallization peak, the artifacts originating from the preceding heating process were eliminated by baseline correction. For correction, the DSC curves were divided into three regions: (1) the artifact region, (2) the crystallization peak region, and (3) the plateau region. The artifact and plateau regions were individually fitted to reproduce the baseline, while a straight line connecting both sides of the fitted curves was used as the baseline across the crystallization peak.

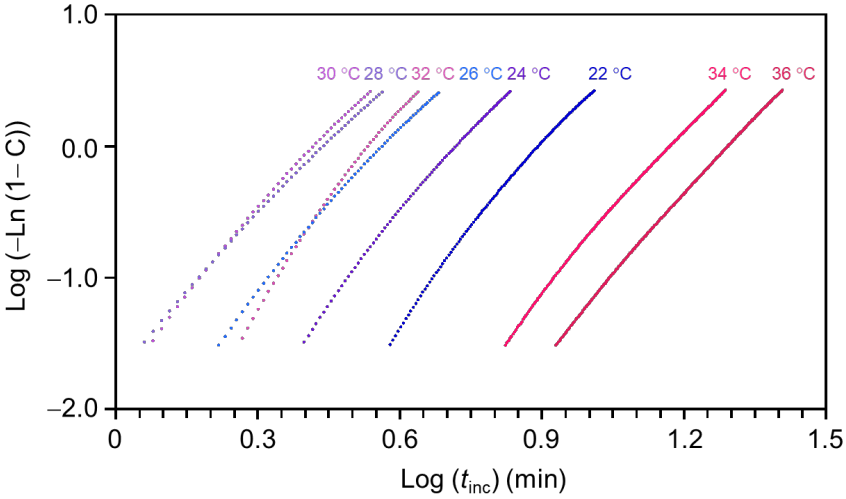

Supplementary Fig. 16.
Avrami plots of **Chol-C$_{12}$** derived from the data presented in **Supplementary Fig. 15**.

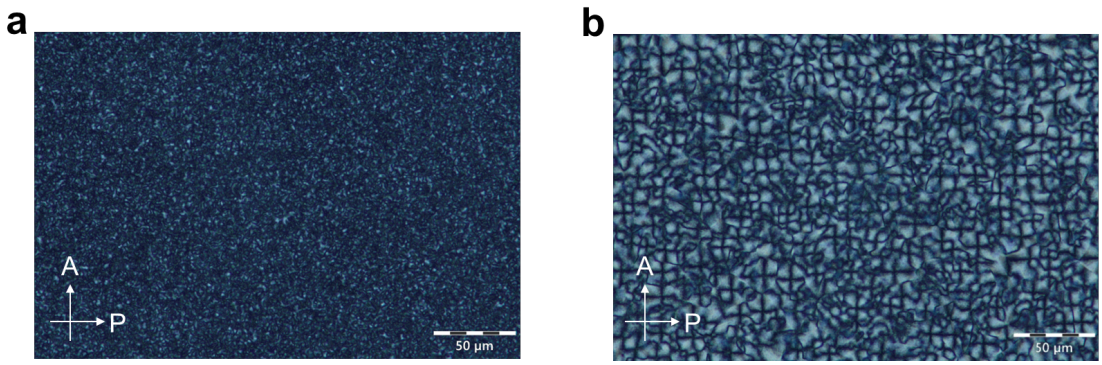

Supplementary Fig. 17.
a,b, Polarized optical microscopy images of **Chol-C$_{12}$** quenched to ambient temperature and subsequently aged for 0 min (a) and 1 day (b), showing the progressive formation of spherulites: scale bar = 50 µm.

S3g. Viscosity of Chol-C_{12}

To measure the viscosity of the undercooled LC **Chol-C_{12}**, a **Chol-C_{12}** sample was first melted at 100 °C on a disposable dish and then subjected to either deep quenching (−196 °C) or shallow quenching (25 °C). A shear deformation at a rate of 30 s^{-1} was subsequently applied to the undercooled LC **Chol-C_{12}** at 25 °C. As shown in **Supplementary Fig. 18**, the viscosity of deeply quenched **Chol-C_{12}** increased from 10^6 mPa·s to 10^7 mPa·s after about 200 s due to crystallization. In contrast, the viscosity of the shallowly quenched sample remained nearly constant throughout the experimental period, reflecting a much longer crystallization kinetics.

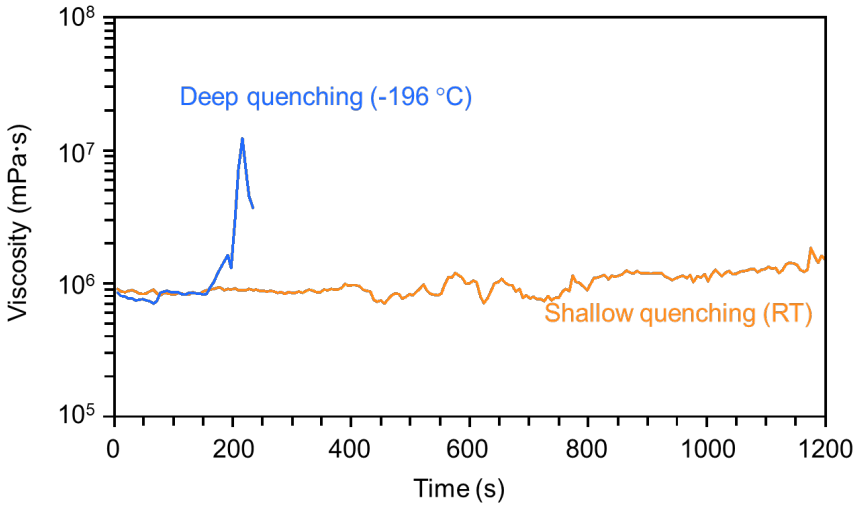

Supplementary Fig. 18.

Viscosity of **Chol-C_{12}** under deep quenching (−196 °C, blue line) and shallow quenching (25 °C, orange line) conditions.

S3h. Selective reflection by the chiral smectic phase of Chol-C_{12}

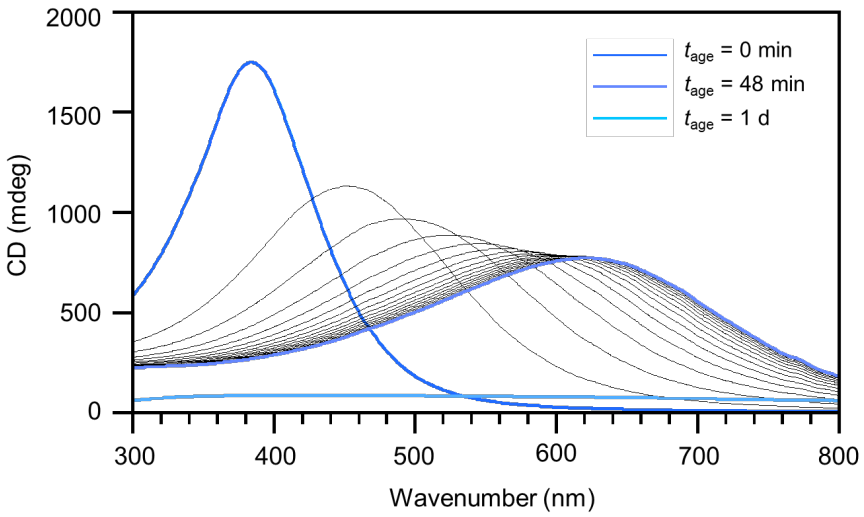

Supplementary Fig. 19.
Time-dependent CD spectra of **Chol-C_{12}** recorded at 3-min intervals from 0 to 48 min, with an additional spectrum collected after 24 h.

The colour information in the real-time video was quantified using the hue parameter. The video was sampled every 20 s, and the region of interest from each extracted frame was converted from RGB (red, green, and blue) to the hue color space in ImageJ (Fiji). The mean hue value of each frame was then obtained and used for subsequent analysis.

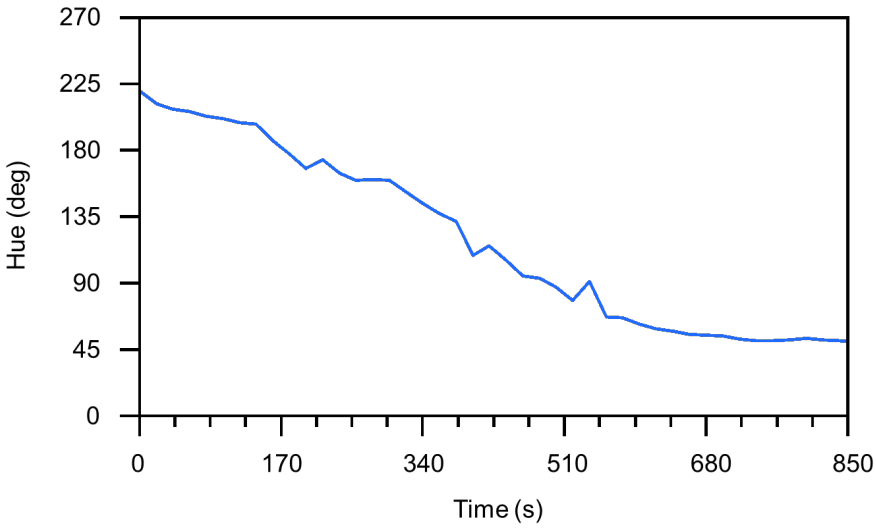

Supplementary Fig. 20.
Temporal variation in hue degree over a period of 14 min, indicating the disappearance of the selective reflection of chiral smectic LC phase upon crystallization.

S3i. Comparison with another cholesteryl compounds

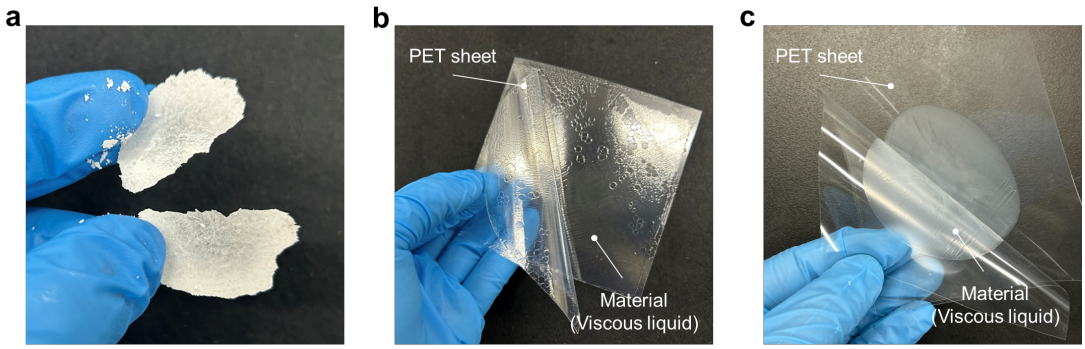

Supplementary Fig. 21.
a-c, Cholesterol (a), cholesteryl oleyl carbonate (b), and a simple mixture of cholesterol and cholesteryl oleyl carbonate (1/1 in mol%) (c) were prepared under the same conditions as **sheet-0**. None of these materials were able to form a free-standing sheet.

S3j. Appearance of sheets

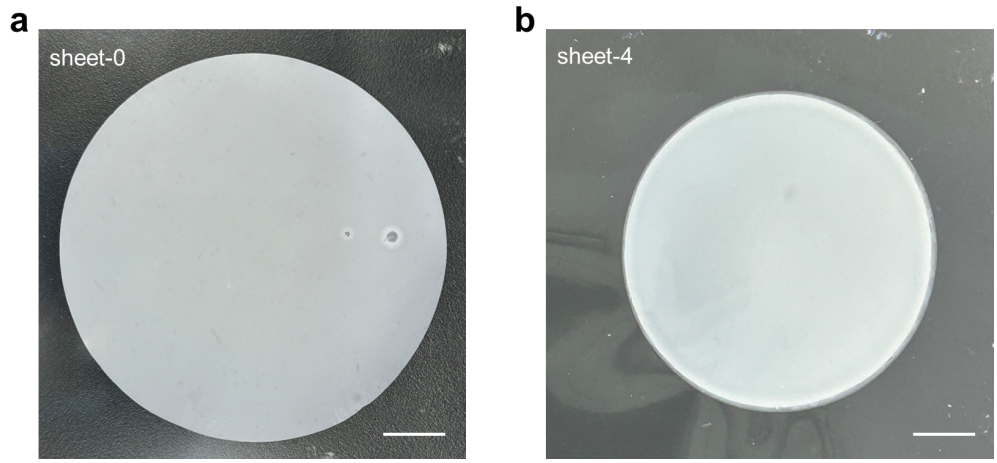

Supplementary Fig. 22.
a,**b**, The appearance of **sheet-0** (a) and **sheet-4** (b): scale bar = 2 cm.

S3k. Molecular alignment in another sheets

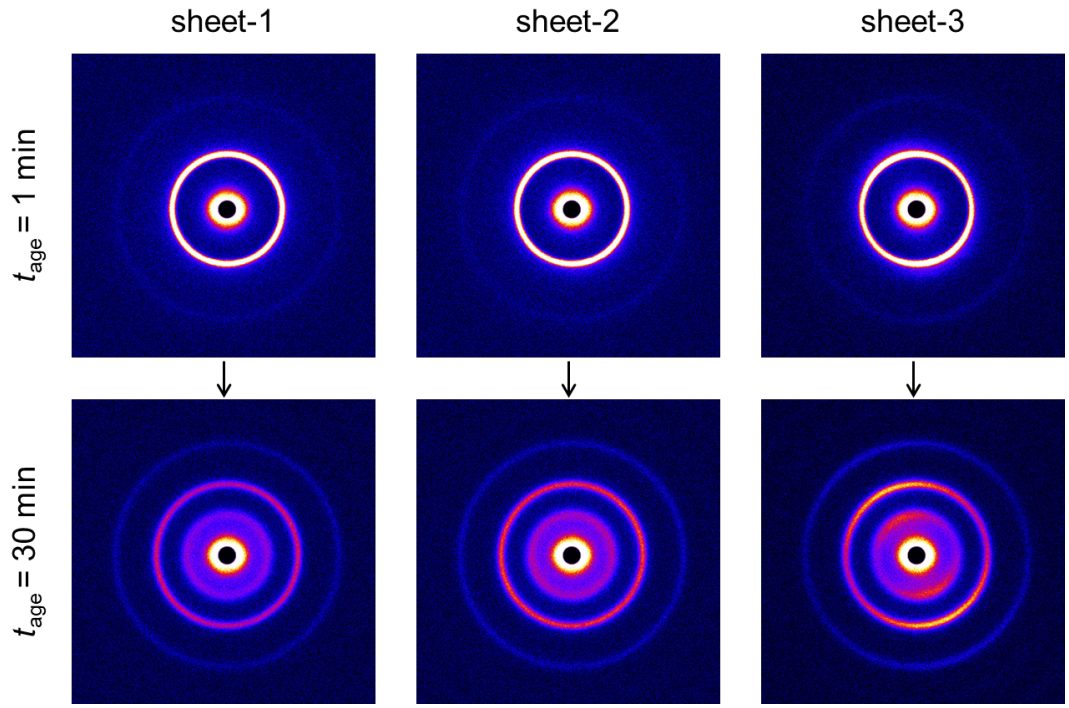

Supplementary Fig. 23.
2D-XRD images of **sheet-1**, **sheet-2**, and **sheet-3** obtained immediately after pressing (t_{age} = 1 min) and after subsequent aging (t_{age} = 30 min), upon exposure to an X-ray irradiation perpendicular to the sheets.

S3l. Macroscopic view of the molecular alignment in sheet-4.

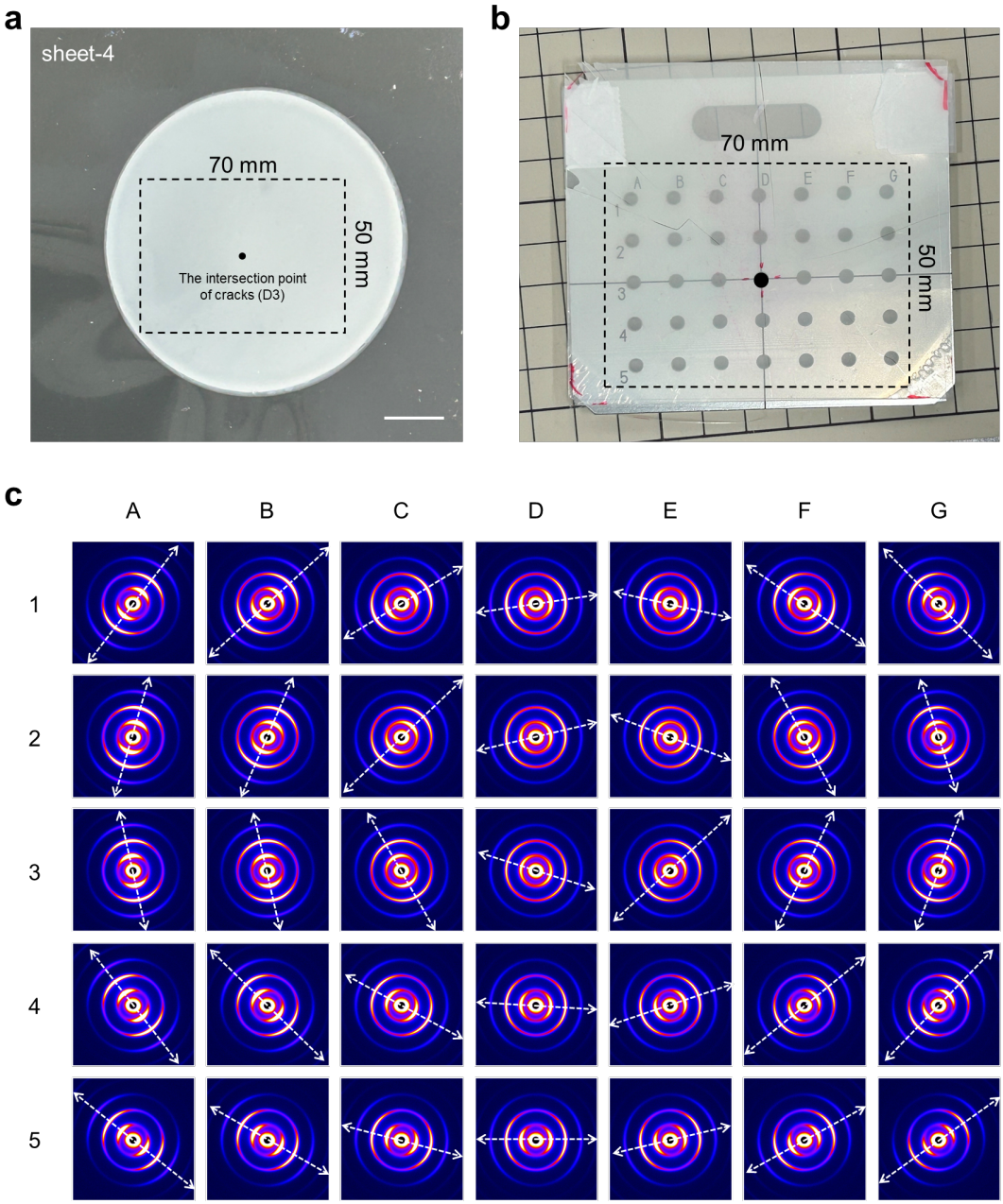

Supplementary Fig. 24.
a,**b**, After aligning the intersection point of cracks in **sheet-4** with the D3 position of the XRD sample stage (a), a **sheet-4** was measured by 2D-XRD mapping measurement at 35 positions (7 × 5 grid) (b). As shown in **c**, the lamellar structures exhibit an orientation along the tangential direction, indicating that the molecular alignment follows the flow direction.

S3m. Tensile testing results of sheet-0 and sheet-4

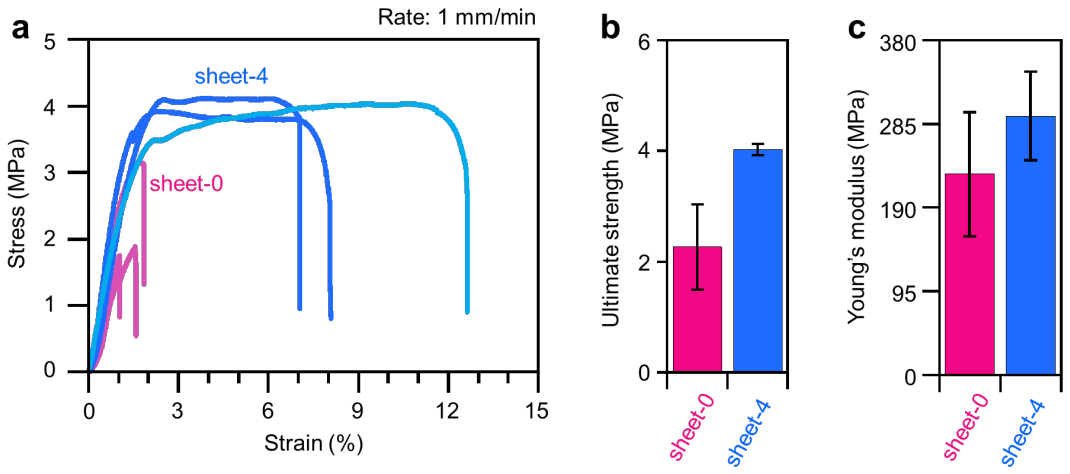

Supplementary Fig. 25.
a, Tensile stress–strain curves of **sheet-0** and **sheet-4**, each obtained from three independent specimens (n = 3). **b**, Summary of the ultimate stress values. The non-oriented **sheet-0** exhibits a larger standard deviation and a lower ultimate stress compared to the highly oriented **sheet-4**. **c**, Young's modulus of **sheet-0** and **sheet-4**. The enhanced molecular alignment in **sheet-4** results in a significantly higher modulus.

S3n. Tensile testing results after environmental moisture exposure

To generate a high-humidity environment,[S2] the prepared **sheet-4**, a hygrometer, and a container of saturated brine were placed inside a transparent acrylic chamber. A brief vacuum (~30 s) was applied until the saturated brine began to boil, after which the vacuum was stopped applying. The humidity subsequently increased and stabilized at approximately 84%. **Sheet-4** was kept under this high-humidity environment for one day, then subjected to tensile testing.

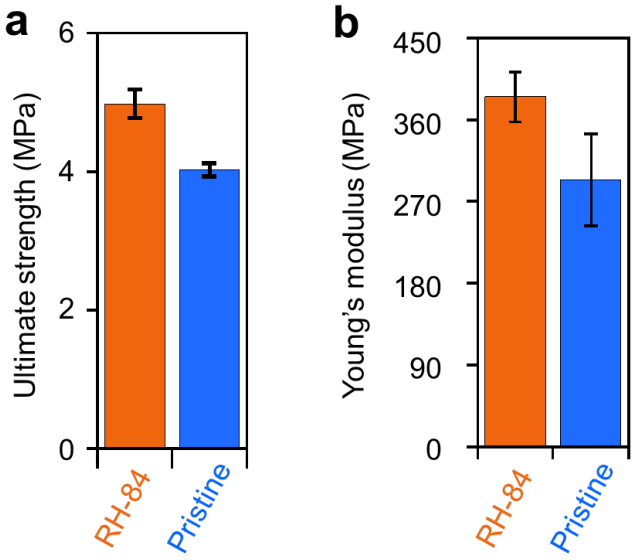

Supplementary Fig. 26.

a,**b**, Ultimate stress values (a) and Young's modulus of **sheet-4** (RH-84 and pristine) (b). These results show that the mechanical properties of **Chol-C_{12}** exhibit only minimal changes under environmental humidity, demonstrating its durability against moisture exposure.

S3o. Recyclability of Chol-C_{12}

A part of **sheet-4** was placed in a sample vial, dissolved in 1 mL of $CDCl_3$, and analyzed by ^1H NMR spectral measurement (400 MHz)**.**

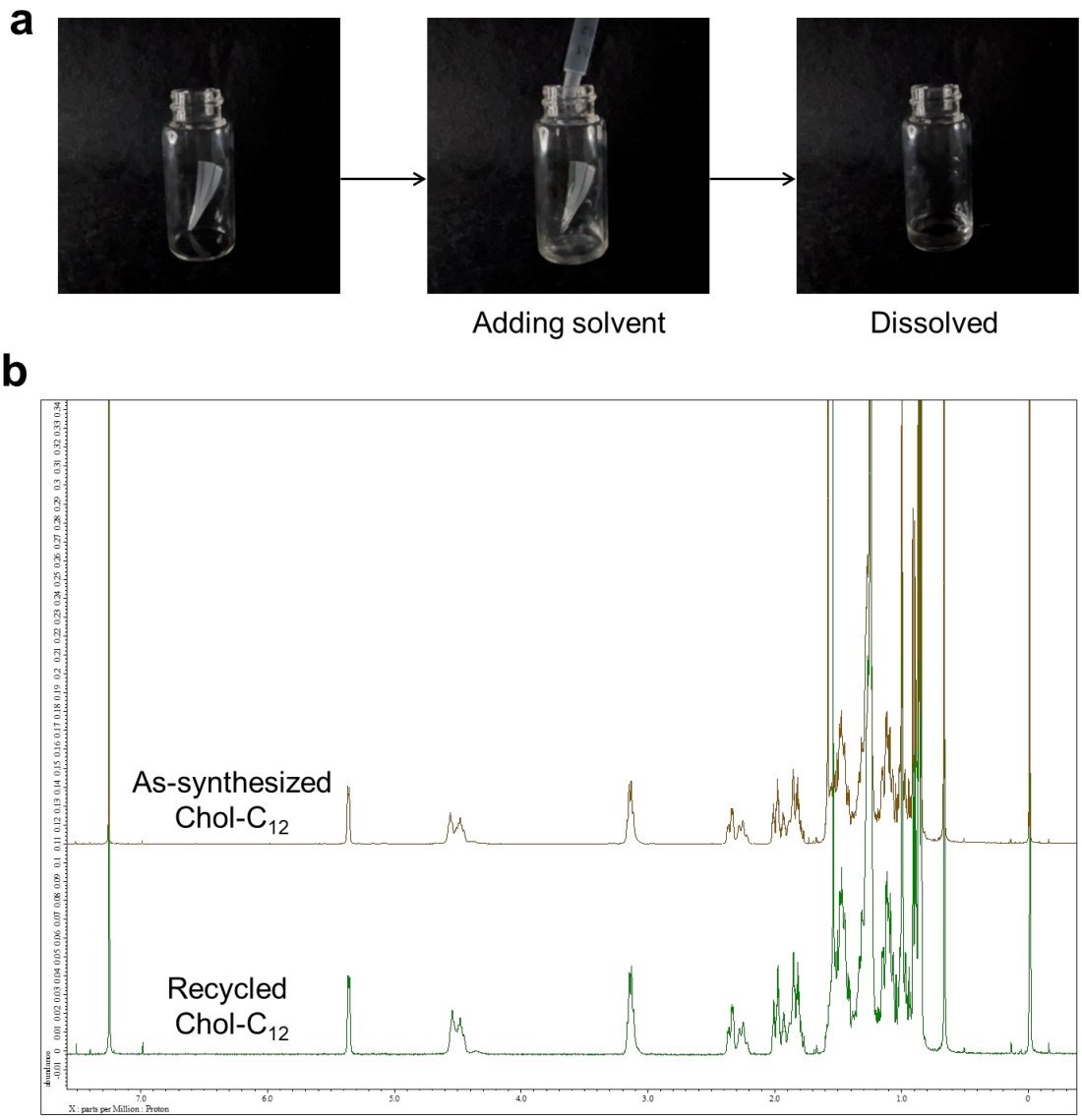

Supplementary Fig. 27.

a, The process of recycling **sheet-4**. **b**, ^1H NMR spectra (400 MHz) of a recycled **Chol-C_{12}** from a processed **sheet-4** (green line) and as-synthesized **Chol-C_{12}** (brown line) in $CDCl_3$ at 298 K.

S3p. "Hibernation" of metastable LC Chol-C_{12}

A **Chol-C_{12}** sample was first heated to 100 °C above its melting point to eliminate thermal history if any. It was then rapidly quenched to −50 °C at 50 °C/min and maintained for 1 day to kinetically arrest the material in a LC glassy state. Upon subsequent heating to 30 °C followed by a 1 h incubation, crystallization emerged, indicating that **Chol-C_{12}** remains vitrified and unable to undergo crystallization when held below its glass-transition temperature.

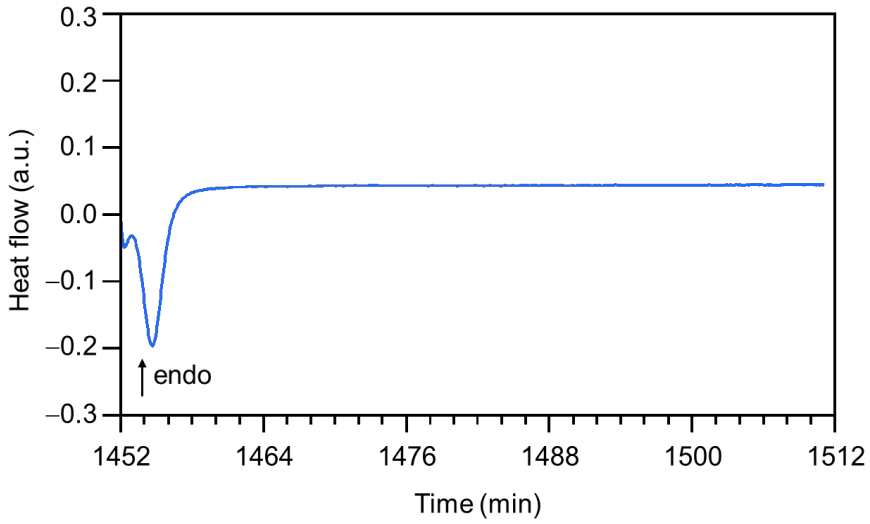

Supplementary Fig. 28.

Isothermal DSC curve of the **Chol-C_{12}** sample incubated at 30 °C for 1 h after being previously frozen at −50 °C for 1 day (1440 min).

S3q. Tensile testing results of Chol-C_{12} filaments

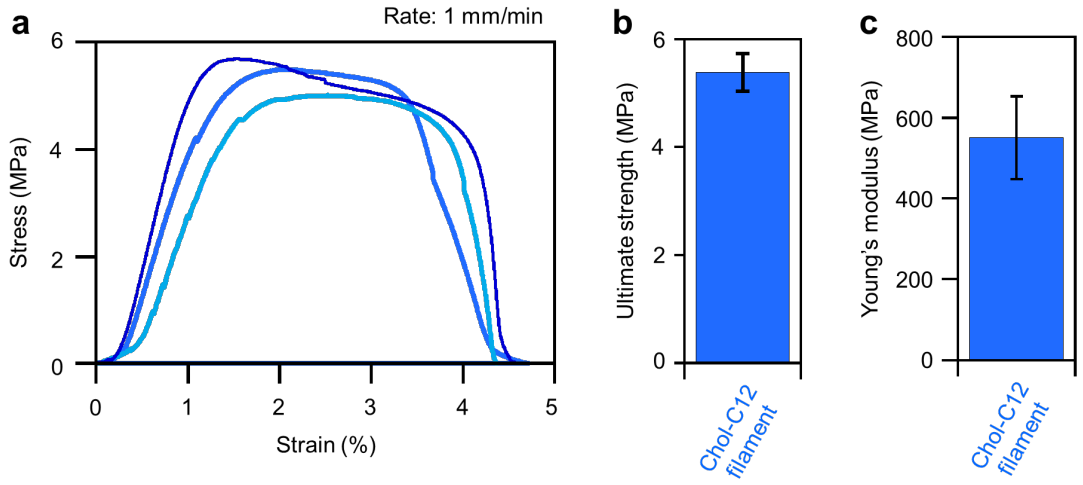

Supplementary Fig. 29.
a, Tensile stress–strain curves of **Chol-C_{12}** filament, each obtained from three independent specimens (n = 3). **b**,**c**, Summary of the ultimate stress values (b) and Young's modulus (c).

S4. Reference

S1. Avrami, M. Kinetics of phase change. I. General theory. *J. Chem. Phys.* **7**, 1103–1112 (1939).

S2. Young, J. F. Humidity control in the laboratory using salt solutions—A review. *J. Appl. Chem.* **17**, 241–245 (1967).